LA-UR-16-27438 (Accepted Manuscript)

Vortex Flux Dynamics and Harmonic ac Magnetic Response of Ba(Fe0.94 Ni0.06)2As2 Bulk Superconductor

Nikolo, Martin
Zapf, Vivien
Jiang, Jianyi
Singleton, John
Hellstrom, Eric
Weiss, Jeremy

To be published in: Journal of Superconductivity and Novel Magnetism

DOI to publisher's version: 10.1007/s10948-016-3618-8

Permalink to record: http://permalink.lanl.gov/object/view?what=info:lanl-repo/lareport/LA-UR-16-27438

Vortex flux dynamics and harmonic ac magnetic response of $Ba(Fe_{0.94}Ni_{0.06})_2As_2$ bulk superconductor

Martin Nikolo[1], Vivien S. Zapf[2], John Singleton[2], Jianyi Jiang[3], Jeremy Weiss[3], and Eric Hellstrom[3]

[1]Department of Physics, Saint Louis University, St. Louis, MO 63103, USA, nikolom@slu.edu, telephone: +1 (314) 717-1784.
[2]National High Magnetic Field Laboratory, Los Alamos National Laboratory, Los Alamos, NM 87545, USA.
[3]Applied Superconductivity Center, National High Magnetic Field Laboratory, Florida State University, Tallahassee, FL 32310, USA

Vortex dynamics and non-linear ac response are studied in a $Ba(Fe_{0.94}Ni_{0.06})_2As_2$ (T_c = 18.5 K) bulk superconductor in magnetic fields up to 12 T via ac susceptibility measurements of the first 10 harmonics. A comprehensive study of the ac magnetic susceptibility and its first ten harmonics finds shifts to higher temperatures with increasing ac measurement frequencies (10 to 10,000 Hz) for a wide range of ac (1, 5, and 10 Oe) and dc fields (0 to 12 T). The characteristic measurement time constant t_1 is extracted from the exponential fit of the data and linked to vortex relaxation. The Anderson-Kim Arrhenius law is applied to determine flux activation energy E_a/k as a function dc magnetic field. The de-pinning, or irreversibility lines, were determined by a variety of methods and extensively mapped. The ac response shows surprisingly weak higher harmonic components, suggesting weak non-linear behavior. Our data does not support the Fisher model; we do not see an abrupt vortex glass to vortex liquid transition and the resistivity does not drop to zero, although it appears to approach zero exponentially.

I. Introduction

The recent discovery of oxygen-free, iron-pnictide superconductors has greatly enriched superconductivity research, creating a second class of high-temperature superconductors besides the cuprates. Fe-pnictides are layered with electronically active Fe-As layers alternating with buffer layers of different chemical composition.[1,2] Iron pnictides are metallic with a multiband electronic structure, while cuprates are strongly correlated Mott insulators with single band behavior.[3-7] But most importantly, the coexistence of magnetism and superconductivity on a nanoscale level for the Fe-based systems is significantly different than in the cuprates. Ni-, K-,

and Co-doped $BaFe_2As_2$ (also known as 122 materials) show rather small anisotropy, high critical field H_{c2}, and large robustness of the critical current as a function of the magnetic field.[3,8]

In order to enhance the current-carrying capacity of bulk materials, it is essential to study the magnetic vortex and vortex pinning behavior to understand the underlying mechanism causing the rapid decrease of the critical current densities with magnetic field. Grain boundaries, twinning planes, inhomogeneities in composition, normal regions, voids and cracks can act as pinning sites. However, if the size of these defects is not comparable to the coherence length, the grains can decouple and severely suppress the critical current capacity.[9-12]

Ac susceptibility measurements are versatile because they probe regions of $E - j$ (electric field–current density) phase space that are not easily accessible to transport measurements. They reveal the magnetic response of the superconductor both in linear as well as nonlinear regimes. The high sensitivity of the ac susceptibility technique allows us to investigate the low voltage region in the $I - V$ (current–voltage) characteristics.

States with irreversible magnetic properties produce nonlinear $I - V$ characteristics, which also induce nonlinearities in the magnetic response of the sample, giving rise harmonics higher than the first one. We study flux dynamics, flux pinning, and higher harmonics in the ac magnetic response of the bulk superconductor $Ba(Fe_{0.94}Ni_{0.06})_2As_2$ (T_c = 18.5 K).

In a bulk sample, grains and grain boundaries are connected by junctions that are connected in a complicated series and parallel arrangement. Far below T_c the grains are coupled and the induced current from the external ac magnetic field results in shielding currents along the sample's outermost surface. Below T_c, the first harmonic response of the imaginary part of ac susceptibility, χ_1'', on a $\chi_1'' - T$ plot, exhibits a broad peak that is attributed to hysteresis losses. As temperature increases toward the critical temperature T_c from below, flux lines and bulk shielding currents penetrate the sample when the measuring field exceeds the lower critical field. When the flux lines and shielding currents fully penetrate the material, the losses reach a maximum. As the temperature increases beyond T_c, the shielding currents recede and the losses drop to zero. These same processes occur around T_c of the grains (intrinsic) or of the grain boundaries (coupling),

however the coupling losses dominate near T_c of the bulk sample.[13]

II. Experimental Details

The first 10 harmonics of ac susceptibility were measured by the Quantum Design PPMS ac susceptometer on polycrystalline bulk superconductor $Ba(Fe_{0.94}\ Ni_{0.06})_2As_2$ (T_c = 18.5 K) (referred to as Ni6) in magnetic fields up to 12 T for 3 ac fields (1, 5, and 10 Oe) and 4 frequencies (10, 100, 1000, and 10,000 Hz). Previously, we also measured resistivity of the sample in fields up to 18 T, magnetization and Proximity Detector Oscillator (PDO) measurements in pulsed fields up to 65 T at the National High Magnetic Field Laboratories in Tallahassee, FL and Los Alamos, NM. Although the focus here is on the ac susceptibility work, whenever it is appropriate we contrast the ac susceptibility data with our previous measurements.

The samples were synthesized at the Applied Superconductor Center (at the National High Magnetic Field Laboratory), where Ba, Fe, Ni and As were mixed and ground together, wrapped with Nb foil, and then sealed in a stainless steel vial. The sealed samples were heat treated under a pressure of 193 MPa at 1120 °C for 12 hours, cooled to 900 °C at the rate of 4 °C/hr, held at 900 °C for 12 hr, and then cooled to room temperature at 150 °C/hr. The phase purity of the samples was checked by powder X-ray diffraction (XRD).[14] The samples contained a small amount (a few %) of FeAs impurities. The Ni6 bar-shaped sample had dimensions 0.7 x 0.7 x 2 mm.

The principle of measuring ac susceptibility involves subjecting a sample to a small alternating magnetic field. The sensing coil picks up the flux variation and the resulting induced voltage is detected. This recorded voltage is proportional to the time derivative of the sample's magnetization which can contain higher harmonics. The local flux density B in the sample shows a phase lag behind the applied ac H field. For small applied ac fields, the response is nonlinear in the mixed state. One can observe this by measuring a distorted periodic waveform of the induced voltage. Neither B nor M can be expressed as a sinusoidal function of single frequency and the average local flux density and magnetization $M(t)$ within the sample is described by a Fourier expansion. The method of ac susceptibility measurements including measurements of higher harmonics is described in detail by Goldfarb and Nikolo.[15,16] The ACMS ac susceptibility option

was used in a 14 T Physical Properties Measurement System by Quantum Design. The sample is located in one of two counter-wound sensing coils so as to remove linear backgrounds. A 5-point measurement technique was used, where the sample is measured in each of the two counter wound coils, as well as in neither coil as an additional background subtraction. Finally, a calibration coil centered in each counter-wound sensing coil is measured to correct for phase shifts in the instrumentation and cabling. Thus in phase and out-of-phase signals can be accurately separated.

Ac susceptibility was measured in dc magnetic fields of 0, 2, 4, 6, 10, and 12 T for ac field amplitudes of 1, 5, and 10 Oe and ac field frequencies of 10, 100, 1000, and 10,000 Hz. Figure 1 shows χ_1' and χ_1'' as a function of temperature for different ac and dc fields for f =10,000 Hz.

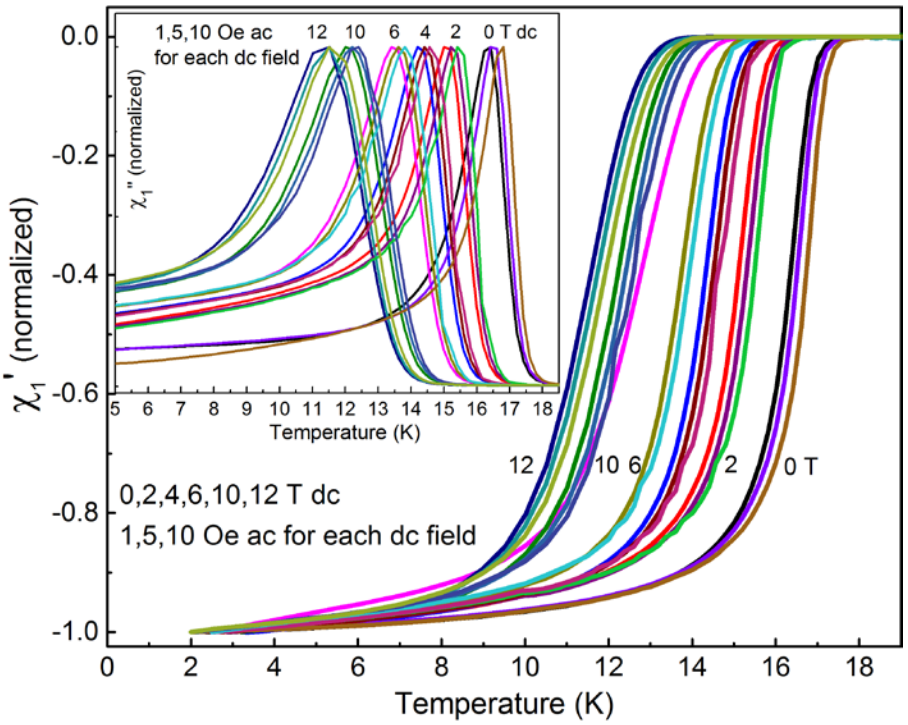

Figure 1. χ_1' and χ_1'' as a function of temperature for different ac and dc fields for f =10,000 Hz.

The selected measurement frequencies correspond to time windows in which the vortex dynamics regimes like flux creep, flux flow and TAFF are detectable. The real part of the first harmonic χ_1'

represents the screening properties of the sample, and it is proportional to the time average of the energy stored in the sample's volume. The imaginary part χ_1'', represents the energy converted into heat during one cycle of the ac field.

III. Results and Analysis

A. Frequency and time dependence

Both χ_1' and χ_1'' shift to higher temperatures for higher ac frequencies. See Figure 2. This frequency shift of the susceptibility curves is observed for all measured ac and dc magnetic fields. At higher frequency, the critical state field profile has less time to relax and therefore the effective pinning force density increases with increasing frequency, causing the ac loss peak in χ'' to shift to a slightly higher temperature. As the temperature increases toward the temperature of the peak, T_p, from below, flux lines and bulk shielding currents penetrate the sample when the measuring field exceeds the lower critical field. The flux penetrates deeper and deeper into the sample and the ac losses increase, finally reaching maximum at T_p where the flux fully penetrates the sample. Also at that time the shielding currents penetrate the center of the pellet. In other words, at a given temperature near the χ_1'', higher frequencies allow less time for flux to penetrate the sample and less time to relax. This tends to improve its shielding ability.[13]

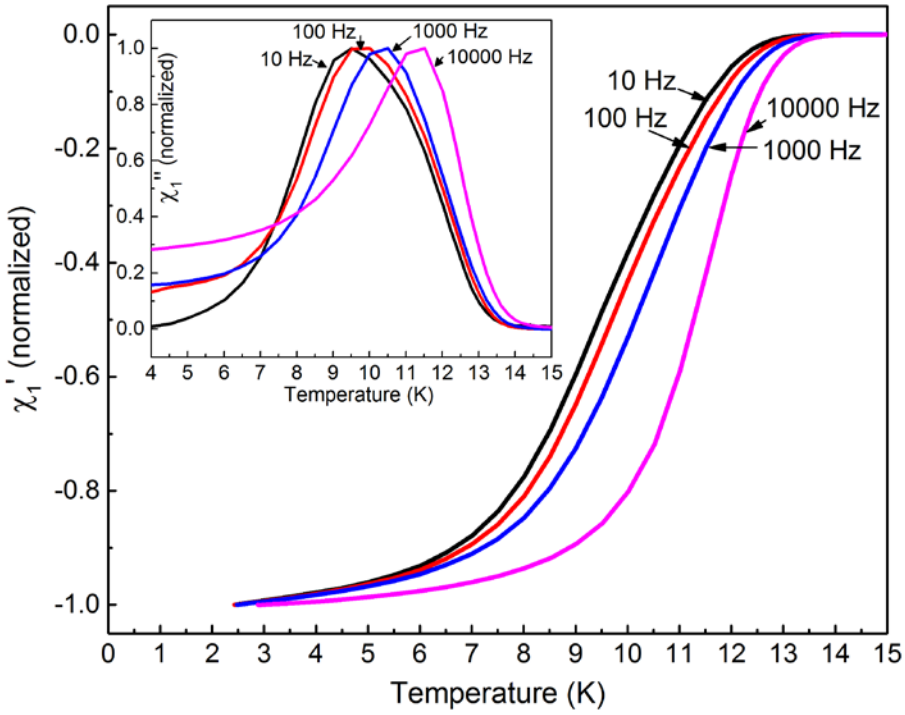

Figure 2. χ_1' and χ_1'' as a function of temperature and frequency for 10 Oe ac and 12 T dc fields.

The frequency shift can be explained by a competition between the Lorentz force and flux pinning force. In the presence of a current density $\boldsymbol{J}$, and the penetrated flux density, $\boldsymbol{B}$, the flux lines experience a Lorentz force per unit volume $\boldsymbol{F_L}=\boldsymbol{J}\times\boldsymbol{B}$, which moves them sideways. The flux motion is resisted by viscous drag and by inhomogeneities in the lattice that pin the flux. For flux lines held in potential wells of depth U and width a, the force acting on the vortex is $F_L V_b$ where V_b is the volume of the flux lattice surrounding each pinning center. The Lorentz force acting on the vortices, causes decrease of the flux de-pinning activation energy, E_a, to an effective height of $U - F_L V_b a$, resulting in more vortices being depinned during each ac field cycle.[17]

At nonzero temperatures, flux motion is possible with the help of thermal activation. The thermally-activated flux bundles hop in the direction of the Lorentz force at a rate of $\upsilon = \upsilon_0[exp(-(U - F_L V_b a)/kT) - exp(-(U + F_L V_b a)/kT)]$ where υ_0 the attempt frequency for hopping, and υ the flux line hopping rate. The backward hopping term can be neglected since the larger Lorentz

force density makes the second term in above equation much smaller and one can rewrite above the equation as $F_L=F_p=(1/aV_b)[(U + kTln(\upsilon/\upsilon_0)]$ in the critical state.[18]

This means that the pinning force depends logarithmically on the flux hopping rate and therefore, also on the frequency of the driving ac field. Even if the Lorentz force is smaller than the pinning force, some vortices move via thermal fluctuation. This has been named flux creep. In this regime, resistivity is not exactly zero, although very small. Maximum dissipation occurs when the driving frequency matches the vortex hopping frequency.

The flux creep of the vortices over pinning centers induces dissipation and reduces the critical current density j_c. For a one-dimensional case, at a given temperature, $dH/dx = j_c = F_p/|B(x)| = j_0 +$ const ln υ/υ_0, where j_0 is the current density in the absence of flux relaxation.[18] Once the critical state is reached, the hopping rate falls below a practically observable limit and $\upsilon/\upsilon_0 << 1$. The ln term is negative and the slope of the flux profile and therefore the critical current density decreases or relaxes.

The flux creep begins at the beginning of the measurement and at time $t = 0$ it is very large. As time goes on, this creep rate slows down and at some time later, t_s, it is no longer observable and steady state is reached. Thus time t_s is needed for the flux profile to reach steady state. For a lower driving frequency, the sample 'sits' in any given value of the applied ac field longer and the flux lines have more time to continue to relax.[17]

Figure 3 plots T_p as a function of frequency for ac fields of 1, 5, and 10 Oe, and two selected dc fields of 2 and 4 T. The inset graph plots T_p as a function of measurement time frame $t=1/f$ for all measured dc fields of 0, 2, 4, 6, 10, and 12 T, in addition to the three ac fields of 1, 5, and 10 Oe. The data show that below approximately 1000 Hz, the frequency shift in T_p is relatively significant. Above that frequency, the plot flattens. We fit all the curves with an exponential function $T_p = A_1\exp(-f_1/f) + T_1$ for some fitting constants A_1, f_1, and T_1. The f_1 frequency represents a point on the plot where 66% of the T_p increase occurs relative to the asymptotic value at f = 10,000 Hz. We obtained a fairly narrow f_1 range of 900 Hz < f_1 < 1400 Hz.

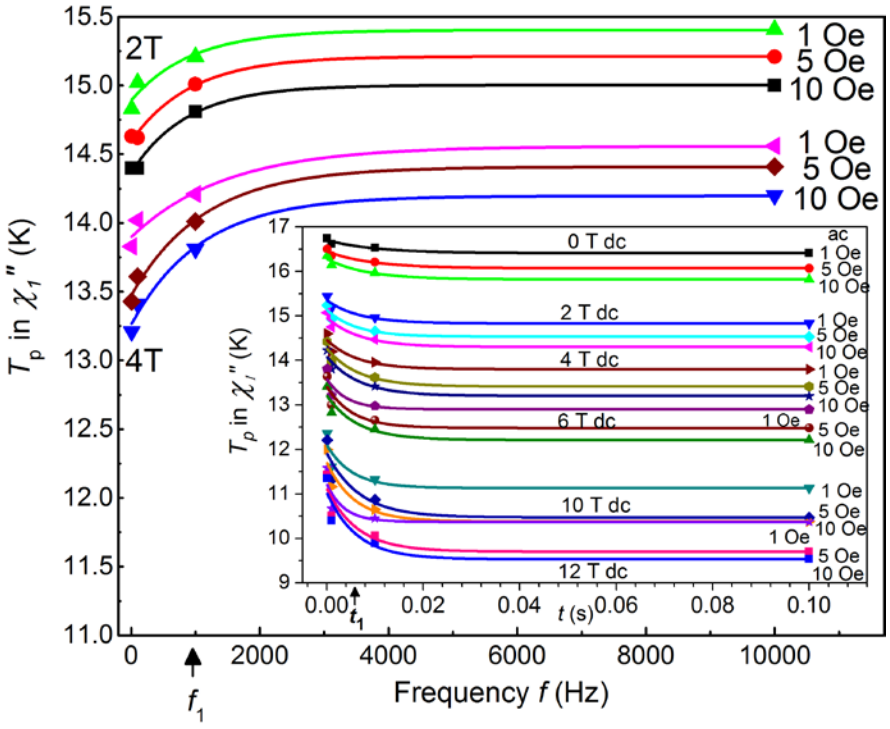

Figure 3. T_p as a function of frequency and T_p as a function of measurement time in the inset graph. f_1 and t_1 fitting constants and are pointed out in the graphs.

We apply similar fitting function to the time-dependent data: $T_p = A_2\exp(-t_1/t) + T_2$, for fitting constants A_2, t_1, and T_2. Now the t_1 characteristic time constant takes on similar meaning as f_1 but it may be more useful because after time equal to, at least, $3t_1$, T_p levels. This means that if our time frame of measurement is smaller than $3t_1$, the vortices do not have enough time to relax and "creep" which leads to higher T_p and therefore "improved" superconducting properties in any ac susceptibility measurement. This suggests that the optimal measurement frequency should be near 100 Hz or less to avoid artificially enhancing the ac susceptibility signal. However, when the sample size is small or the coils are not sensitive enough, one needs to measure at higher ac field frequencies to improve the signal strength which is proportional to frequency. The frequency plot in Figure 3 is not specific just to this sample but similar results have been obtained for a number of other bulk pnictide and cuprate superconductors.[19-22]

The thermal activation over the barriers leads to flux-creep resistivity which is nonzero at any positive temperature, even in the limit of zero current, as the Arrhenius law describes the hopping

rate and the resistivity in the Anderson-Kim model. As mentioned previously, maximum dissipation occurs when the driving frequency matches the vortex hopping frequency. At that temperature we apply the Arrhenius Anderson-Kim model describing the thermally activated vortex hopping: $f = f_0 \exp(-E_a/kT)$, where k is the Boltzmann's constant, f_0 is characteristic frequency, and E_a is the activation energy.[25,26] The inset to Figure 4 shows a cumulative plot of ln f as a function of $1/T_p$ for all measured ac fields and selected dc magnetic fields of 0-10 T. For lower fields of 0 and 2 T, the linearity is evident. However, at higher dc fields, especially above 10 T, there is a distinct breakdown of the linearity and the Anderson-Kim model is only approximate.

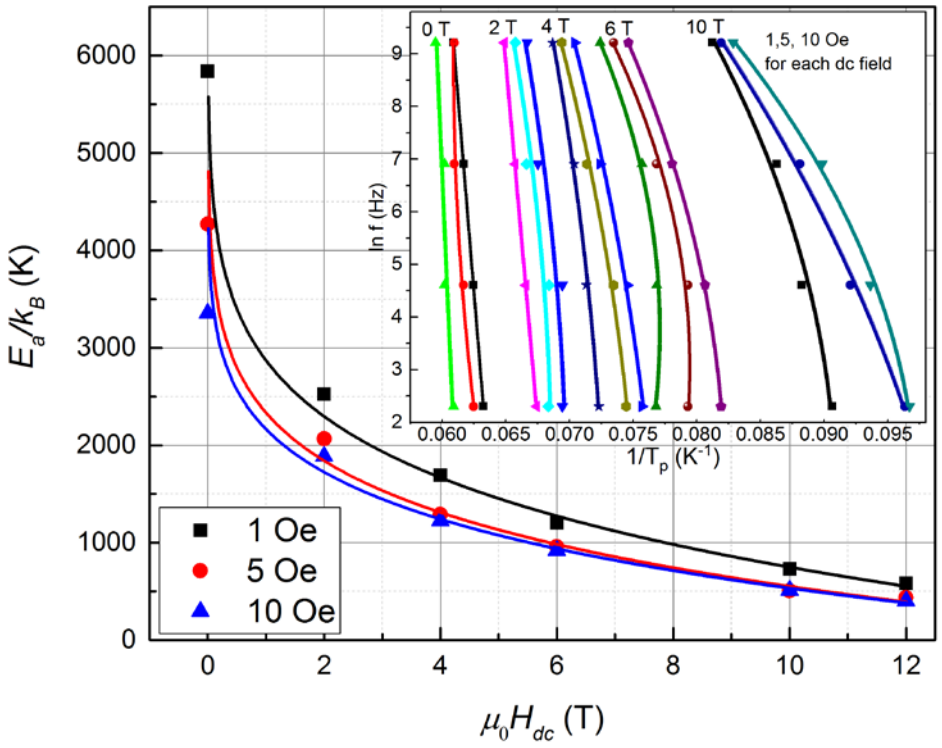

Fig. 4. Plot of activation energy E_a/k_B (K) as a function of dc magnetic field $\mu_0 H_{dc}(T)$ for constant ac field amplitudes. Solid lines are power law fits of E_a/k_B (H_{dc}). The inset graph shows the measurement frequency in ln [$f(Hz)$] as a function of inverse χ_1'' peak temperature, $1/T_p$ (K^{-1}), for different ac and dc fields.

Figure 4 shows E_a/k_B as a function of $H_{dc}(T)$. E_a/k begins at 5839 K at $\mu_0 H_{dc}$ = 0 T and H_{ac} = 80 A/m (1 Oe), and then drops very quickly in a non-linear manner as H_{dc} increases, to 582 K at 12 T. We fit the data by a power-law fit E_a/k = const. $\times H_{dc}^{\,b}$, yielding b = 0.13 for H_{ac} = 80 A/m (1 Oe), b = 0.10 for H_{ac} = 400 A/m (5 Oe), and b = 0.13 for H_{ac} = 800 A/m (10 Oe). Similar power law fits were obtained for $(Ba_{0.6}K_{0.4})Fe_2As_2$ and $Ba(Fe_{0.91}Co_{0.09})_2As_2$ bulk superconductors.[20,21]

The temperatures at which the first harmonic χ_1'' peaks, T_p, and the third harmonic χ_3'' peaks, T_{p3}, for different ac fields H_{ac}, frequencies f, and dc fields $\mu_0 H_{dc}$ are shown in Figures 5 and 6. The inset to Figure 6 shows that χ_3'' has an inverted, negative, peak where χ_1'' has positive peak. The values of T_p and T_{p3} approximately overlap across all measured fields and frequencies. Selected data points are fitted with lines to improve the visualization. Here we do not see any obvious inflection point separating the inter- and intra- granular properties as we saw in a $(Ba_{0.6}K_{0.4})Fe_2As_2$ (T_c = 38.3 K) bulk superconductor.[21] The data shows that T_p decreases by approximately 0.4 K for each 1 T increase in the dc field for 80 A/m (1 Oe) ac field amplitude and by 0.5 K/T for 800 A/m (10 Oe).

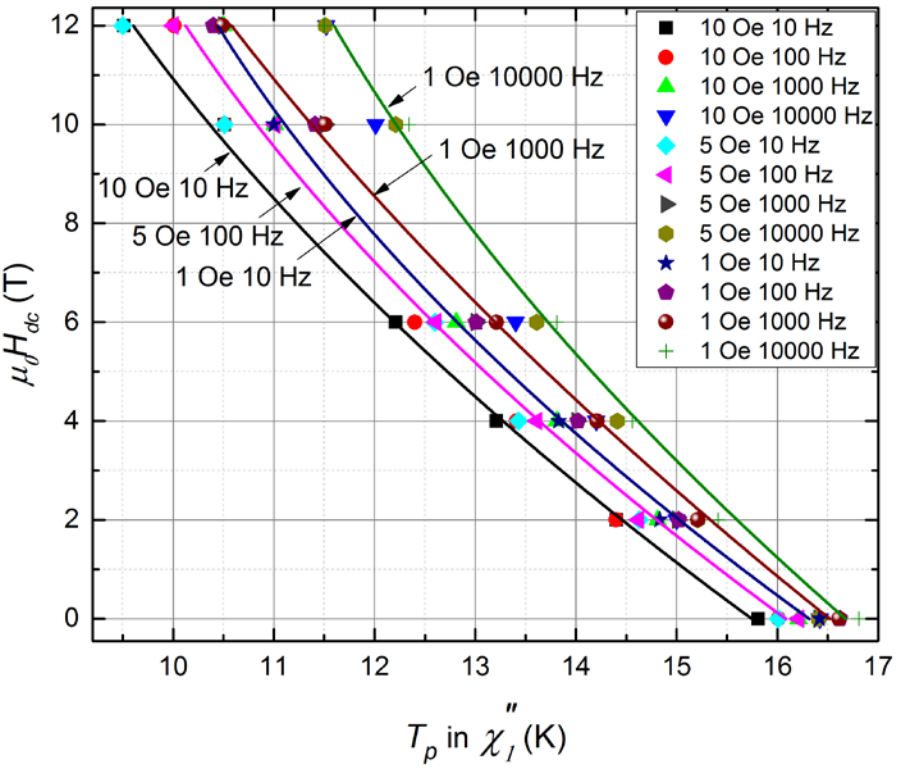

Figure 5. Dc magnetic field $\mu_0 H_{dc}(T)$ vs. the temperature, T_p (K), at which χ_1'' has a peak for different ac driving fields and frequencies.

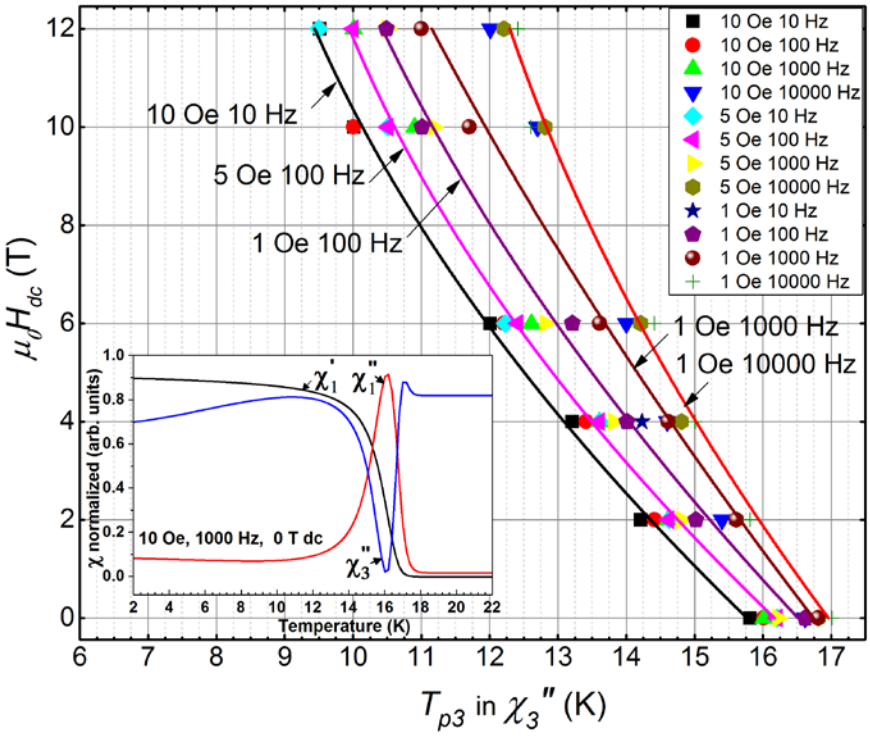

Figure 6. See figure 5 caption. The data is very similar to T_p in Figure 5.

The maxima in χ_1'' and χ_3'' have been used as the definition of the irreversibility temperature (IL).[27-32] This is an alternate method to magnetization measurements. Above the IL line, at higher temperatures and fields, the magnetization of the sample is history-independent, while under the line the sample shows irreversibility. The IL line is the dividing line in magnetic field-temperature phase space between a true superconducting vortex glass region, where the flux lines are pinned and the current is carried without dissipation, and a vortex liquid region where the flux lines move in response to the applied current and the resistance is ohmic. Magnetic irreversibility implies persistent currents and zero resistance. If a narrow temperature interval separating irreversibility and the second upper critical field lines (representing flux flow regime or a vortex liquid state) is ignored, then irreversibility line can be considered as a lower boundary of $H_{c2}(T)$ line.

The lines in Figures 5 and 6 are suggested as our irreversibility lines. However, these lines are broadened by temperature and we don't see any evidence of an abrupt flux transition.

Figure 5 indirectly provides information about the shielding macroscopic current density. The peak in χ_1'' occurs when the ac field just penetrates the center of the sample. At that point we have a field gradient resulting in a field drop H_{ac}, ac field amplitude, from the outside to the center of the sample. This gives us a shielding macroscopic current density $j_m = H_{ac}/R$ where R is the radius of the sample.[23,24] If we model the sample as a long cylinder of radius R = 0.35 mm, we get j_m = 23 A/cm^2 for H_{ac} = 80 A/m and j_m = 230 A/cm^2 for H_{ac} = 800 A/m, respectively. Thus the Figure 5 lines are also frequency-dependent lines of constant current density and show how the time window of measurement influences the relaxation, or creep, in the shielding current density. Larger time measurement window t ($t < 3t_1$) leads to lower measured shielding current density.

B. Linear and non-linear harmonic response

To understand the harmonic response of our sample exposed to ac fields, we note that χ_1'' is a measure of the total dissipation, linear and nonlinear, while the third harmonic susceptibility modulus, χ_3 is a measure of the nonlinear dissipation only.[36] Therefore, the onset of non-linearity can also be defined from the onset of the third harmonic susceptibility. In the framework of Bean's critical state model this onset coincides with the condition $j_c \sim 0$, which can be considered as a condition defining the irreversibility line. In our data, the onset temperature of χ_1'' closely matches the onset temperature of modulus, χ_3. This suggests that the non-linear components are weak. We examine this hypothesis by analyzing the relative strength of the first 10 harmonics of the measured ac susceptibility.

The modulus of the first harmonic χ_1 dominates all the higher harmonics. The only non-negligible harmonic is the third. We plot the scaled comparison of the third and first harmonic moduli, $|\chi_3|/|\chi_1|$ in Figure 7. It reaches maximum of about 9%, at 17.2 K, well past the χ_1'' peak (at 16.2 K) and near χ_1'' foot where total ac losses approach zero (dashed line).

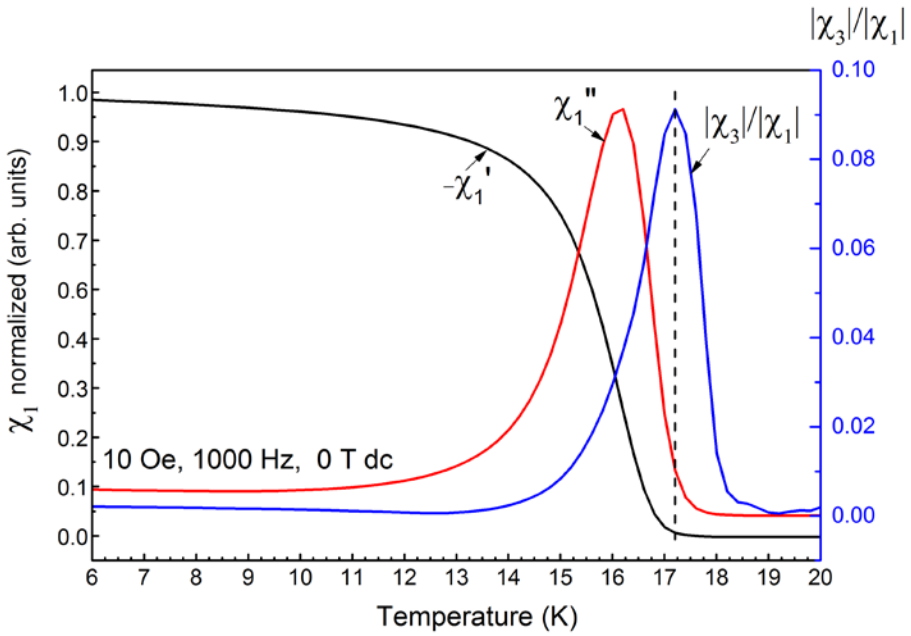

Figure 7. Scaled comparison of the third and first harmonic moduli, $|\chi_3|/|\chi_1|$. We overlap this graph with the χ_1' *and* χ_1'' data to show the superconducting transition. $|\chi_3|/|\chi_1|$ reaches maximum of about 9%, at 17.2 K, well past the χ_1'' peak (at 16.2 K) and near χ_1'' foot where total ac losses approach zero (dashed line).

The second harmonic modulus gives the next-most important contribution. However, it reaches maximum of only 2%, also at 17.2 K. When all harmonic moduli other than the first and third, that is $|\chi_2|$ $|\chi_4|$ $|\chi_5|$, $|\chi_6|$, $|\chi_7|$, $|\chi_8|$, $|\chi_9|$, and $|\chi_{10}|$, are added and compared to $|\chi_1|$, a function similar to $|\chi_3|/|\chi_1|$ in Figure 7, the compared sum peaks at about 8% at 17.2 K.

Although the data shown in Figure 7 are for 0 T, 10 Oe, and 1000 Hz, we analyzed all our data for all measured ac and dc fields, and frequencies, and saw very similar scaling behavior as in Figure 7 and the figure is representative of our other data at other fields and frequencies. The overlap of the $|\chi_3|/|\chi_1|$ with χ_1' *and* χ_1'' in Figure 7 shows that at the superconducting transition, as the temperature increases, and before χ_1'' reaches maximum, the scaled third harmonic is at 3% or less. Also, χ_1' is about 0, or about to turn normal, when $|\chi_3|/|\chi_1|$ peaks. This all somewhat surprising data for we expected stronger non-linearity at lower temperatures.

The data suggests that the ac magnetic response here is largely linear. There is another way to independently check this conclusion. We amplified the induced voltage waveform straight from the secondary coils and captured it on an oscilloscope for several temperatures surrounding the χ_1'' peak. We have done similar work with cuprate bulk samples where we captured the induced and distorted waveforms and used spectrum analyzer to identify the harmonics.[37] Even though our current data was somewhat noisy, the waveforms looked sinusoidal without any major distortions that accompany non-linear behavior along with strong harmonic components seen in cuprates.[37]

C. Fisher vortex glass model

Figures 8 and 9 show the onset of third harmonic modulus χ_3 in the *H*-*T* plane. This onset of the third harmonic susceptibility, χ_3, has been used by many workers[31,38] to determine the vortex melting line, as explained by the Fisher vortex glass theory.[39,40]

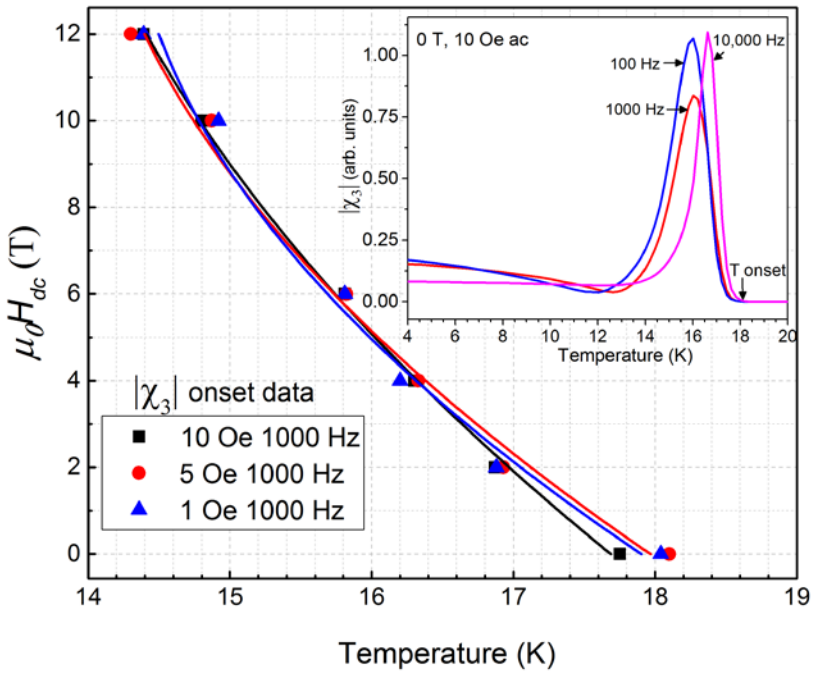

Figure 8. The onset of third harmonic modulus χ_3 in the *H*-*T* plane for f = 1000 Hz. The inset graph shows $|\chi_3|$ vs. *T* for 3 different frequencies at 0 T and 10 Oe ac field. The onset points are frequency independent. The inset arrow shows how the onset was determined.

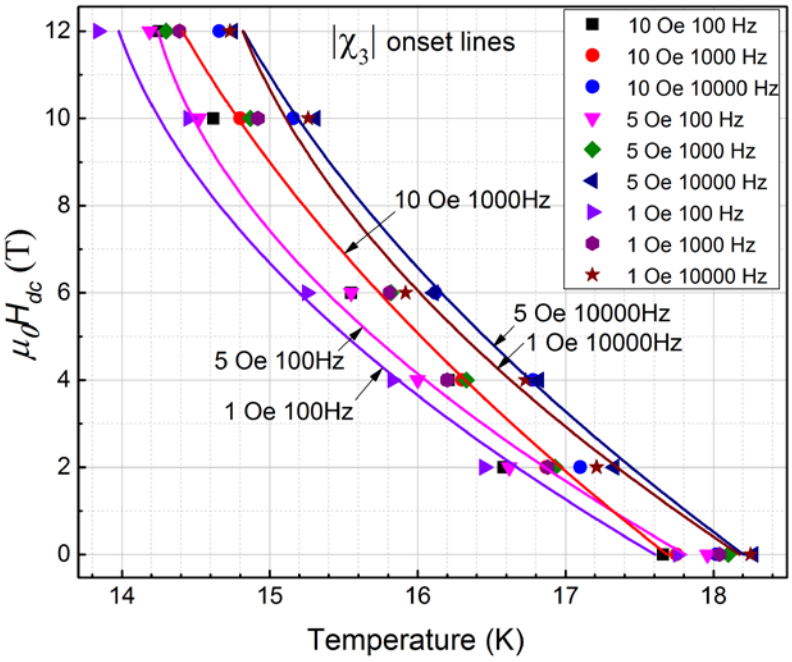

Figure 9. The onset of third harmonic modulus χ_3 in the *H*-*T* plane for different ac fields and frequencies obtained from $|\chi_3|$ vs. *T* graphs. Selected data points were fitted with lines to help visualize the data.

Fisher suggests that with increasing magnetic field H_{dc} the density of flux lines increases, the vortex cores start to overlap, and a new phase, the vortex liquid, appears. In the *H*-*T* plane, this vortex liquid is placed between the irreversibility line and the upper critical field H_{c2}. In the vortex glass (VG) state, below the melting temperature $T_m(B)$, the electric field response to a current density *j* is strongly nonlinear, while for $T > T_m$ (*B*) in the vortex liquid state, it is ohmic for sufficiently low current levels.[39,40]

A vortex liquid phase with nonzero linear resistance experiences a second-order transition to a vortex glass phase with *zero* linear resistance in bulk-disordered superconductors at a well-defined glass-melting temperature T_g. In this model, the system freezes into a genuine thermodynamic amorphous vortex glass phase with some kind of glassy long-range order. The vortex-glass phase is the true superconducting phase with vanishing linear resistivity.[39,40]

This phase change from vortex glass to vortex liquid occurs with only a small DC magnetic field increase at temperatures just below T_c. But it is extremely difficult to discriminate between a true thermodynamic glass and a very slow-moving non-equilibrium viscous vortex liquid (such as window glass), with a small, but nonzero, resistivity due to thermally activated flux creep.

Fischer's model suggests the temperature dependence of the linear resistance R above T_g, scales as $R \sim (T - T_g)^{\nu(z-1)}$ for exponent constants ν and z. This implies that a plot of $(\delta \ln R/\delta T)^{-1}$ vs. T gives a straight line which extrapolates to zero at T_g with a slope $1/\nu(z-1)$.[39,40] The postulated glass temperature T_g is defined as the dividing point between lower temperatures for which the linear resistance is zero (in the limit of very small current), and higher temperatures for which it is not zero.

Our extrapolated glass-melting temperatures T_g's were higher than expected and occurred in the upper part of the resistive transition state of the superconductor.[20] The ac susceptibility and *M-H* data, in addition to our previous resistivity measurements,[19,20] do not support the Fisher model because we do not see an abrupt vortex glass to vortex liquid transition and the resistivity does not drop to zero, although it appears to approach zero exponentially. Rather, the vortex glass to vortex liquid transition is more gradual.

Figure 10 summarizes all our data. It plots the irreversibility lines as derived from χ_1'' peak (1 Oe, 1000 Hz line), *M-H* magnetization, and Proximity Detector Oscillator (PDO) measurements.[33] The overlapping ac susceptibility measurements with the *M-H* data show that they are a reliable method to determine the irreversibility line. The figure further shows the resistivity lines obtained from points near the elbow at 1% of the normal resistance and resistivity obtained at 90% of the normal resistance. The resistivity transition region does not overlap with the χ_1'' T_p line except at 0 T. The resistivity lines are well above the irreversibility lines obtained from *M-H* and ac susceptibility data.

Also, the overlapping onset of third harmonic modulus $|\chi_3|$ (1Oe, 1000 Hz) and the onset of the first harmonic modulus $|\chi_1|$ (1Oe, 1000 Hz) lines are within the resistivity region and therefore unlikely to form melting line boundary as suggested by others.[31,38]

Energy dissipation occurs way below the resistivity elbow and clearly indicates that resistivity is not zero in lower temperatures, even though it may look so on the resistivity vs. temperature graph. This is confirmed by our lower critical field measurements which are near 0 T across full temperature range.[41]

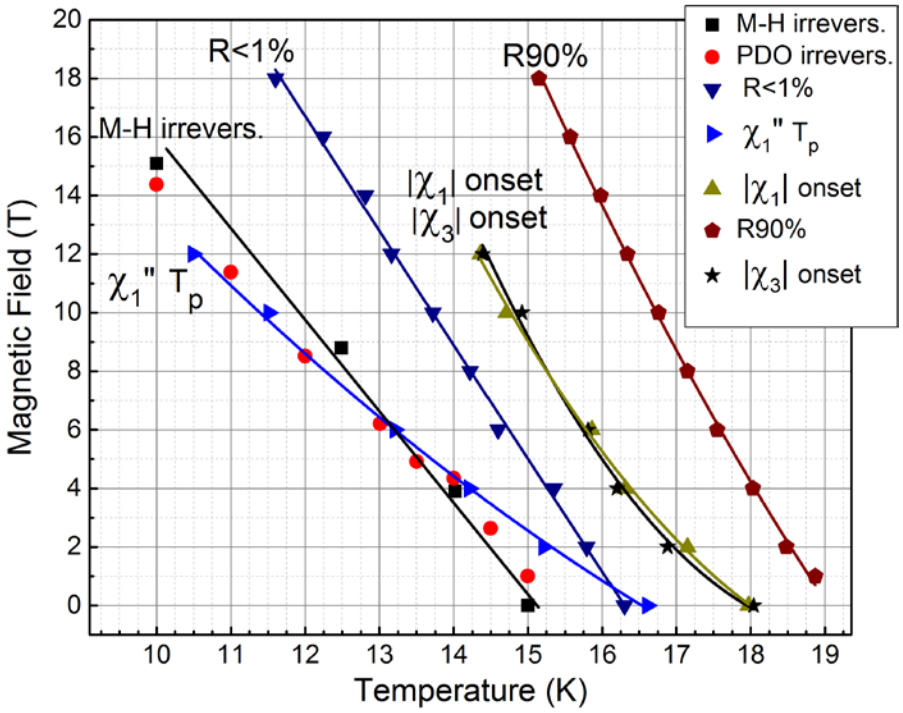

Figure 10. Phase diagram combining all ac susceptibility (1 Oe, 1000 Hz), resistivity, PDO, and magnetization measurements.

IV. Conclusion

A comprehensive study of ac susceptibility curves that shift to higher temperatures with increasing measurement frequencies demonstrate how the time window of measurement impacts the flux relaxation. Time t_s is needed for the flux profile within the sample to reach steady state. For a lower driving frequency, the sample 'sits' in any given value of the applied ac field longer and the flux lines have more time to continue to relax. If the rate of change of the applied

magnetic field is too short, the flux lines do not have time to relax and the transition state moves to a higher temperature, giving an impression of a better superconductor. Our characteristic measurement time constant t_1 extracted from the exponential fit of the frequency data quantifies this vortex-relaxation process and our data show that this relaxation time t_s needs to be at least $3t_1$ for the vortices to settle. In practice, for our ac susceptibility measurements, this suggests using ac field frequency in the 100 Hz range, or lower, to get a true (unshifted) transition curve.

The Anderson-Kim Arrhenius law is applied to determine the flux activation energy E_a/k as a function dc magnetic field. While this model works well for low fields, at higher dc fields, especially at 10 T and higher, there is a distinct breakdown of the linearity in the plot of ln f as a function of $1/T_p$, and the Anderson-Kim model is only approximate. Our results ranged from E_a/k = 5839 K, at 0 T to 582 K at 12 T, and show a quick activation energy drop with increasing magnetic field. We fit a power law to the data: E_a/k = const. $\times H_{dc}^{\,b}$, where b = 0.13.

The ac response shows surprisingly weak higher harmonic components, suggesting strongly linear behavior. The modulus of the first harmonic, χ_1, dominates all the higher harmonics. The only non-negligible harmonic is the third, χ_3, which reaches a relative $|\chi_3|/|\chi_1|$ maximum of 9% only at 17.2 K and for other transition temperatures is very small.

Our data does not support the Fisher model. We do not see an abrupt vortex glass to vortex liquid transition and the resistivity does not drop to zero, although it appears to approach zero exponentially. The presumed vortex glass to vortex liquid transition appears gradual and we observed irreversibility region in the H-T plane.

Acknowledgements

This work was supported by NSF DMR-1006584 and DMR-1306785. The NHMFL facility is supported by the National Science Foundation under DMR-1157490, the State of Florida, and the U.S. Department of Energy

References

1. A.S. Sefat et al., *Phys. Rev. Lett.*, Vol. **101**, 117004, (2008).
2. M. Rotter et al., *Phys. Rev. B*, Vol. **78**, 020503(R), (2008).
3. M.A. Tanatar, *Phys. Rev. B*, Vol. **79**, 094507 (2009).
4. J. Jaroszynski, et al., *Phys. Rev. B*, Vol. **78**, 064511 (2008).
5. Y. L. Chen, et al., *Supercond. Sci. Technol*., Vol. **21**, 115014 (2008).
6. Khasanov, A.; Bhargava, S.C.; Stevens, J.G.; Jiang, J.; Weiss, J.D.; Hellstrom E.E. and Nath, A., *J. Phys. -Condens. Mat.*, **23**, 202201 (2011).
7. G. Celentano, et al., *IEEE Trans. Appl. Supercond*., Vol. **4**, Number 3, June (2011).
8. A. Yamamoto et al., *Appl. Phys. Lett.*, **94**, 062511 (2009).
9. P. Chaudhari et al. Phys. Rev. Lett. 60 1653 (1988).
10. B. Ni et al. Japan. J. Appl. Phys. 27 929 (1988).
11. D. Dimos Phys. Rev. Lett. 61 219 (1988).
12. T. Matsushita et al., Japan. J. Appl. Phys. 27 1658 (1988).
13. Nikolo, M. and R. B. Goldfarb, *Phys. Rev. B*, Vol. **39**, 6615 (1989).
14. Weiss, J. D., Jiang, J., Polyanskii, A. A. & Hellstrom, E. E., *Superconductor Science and Technology* **26,** 074003 (2013).
15. Goldfarb, R.B. et al., *Magnetic Susceptibility of Superconductors and Other Spin Systems*, ed. R.A. Hein, 59, Plenum Press (1991).
16. Nikolo, M., *American. Journal Physics*, Vol. **63**, 57 (1995).
17. Nikolo, M., *Superconductor Science and Technology* **6,** 618 (1993).
18. Müller, K.-H., M. Nikolo, and R. Driver, *Phys. Rev. B*, **43**, 7976 (1991).
19. M. Nikolo, X. Shi, J. Jiang, J.D. Weiss, E.E. Hellstrom, *J. of Superconductivity and Novel Magnetism*, Vol. **27**, Issue 9, 1983-1990 (2014).
20. M. Nikolo, X. Shi, E.S. Choi, J. Jiang, J.D. Weiss, E.E. Hellstrom, *J. of Superconductivity and Novel Magnetism*, Vol. **27**, Issue 10, 2231-2239 (2014).
21. M. Nikolo, X. Shi, E.S. Choi, J. Jiang, J.D. Weiss, E.E. Hellstrom, *J. of Low Temperature Physics*, Vol. **178**, 188-199 (2015).
22. M. Nikolo, X. Shi, E.S. Choi, J. Jiang, J.D. Weiss, E.E. Hellstrom, *J. of Low Temperature Physics*, Vol. **178**, 345-354 (2015).
23. Clem, J.R., Ames Report IS-M 280, "Ac Losses in Type-II Superconductors" (1979).
24. Gomory, F., Takacs, S., Holubar, T., Hilscher, G., *Advances in Cryogenic Engineering*, Vol. **42**, 587 (8), Springer (1997).
25. Anderson, P.W., *Phys. Rev. Lett*., **9**, 309 (1962).
26. Anderson, P.W., and Kim, Y.B., *Rev. Mod. Phys.*, **36**, 39 (1964).
27. Malozemoff, A.P., Worthington, T. K., Yeshurun, Y., Holtzberg, F. H., and Kes, P. H., *Phys. Rev. B*, **38**, 7203 (1988).
28. Gomory, F., Takacs, S., Holubar, T., Hilscher, G., *Physica C*, **235-240**, 2753 (1994).
29. Ishida, T., et al., *Advances in Superconductivity V*, 541 (1993).
30. Deak, J., McElfresh, M., Clem, J. R., Hao, Zhidong, Konczykowski, M., Muenchausen, R., Foltyn, S. and Dye, R., *Phys. Rev. B* **49** 6270(1994).
31. Pissas, M., et al., *Physica C* **476**, 68-72 (2012).
32. Puri, A., et al., *Physics Procedia* **67** 890-895 (2015).
33. Nikolo, M., Singleton, J., Solenov, D., Jiang, J., Weiss, J.D., Hellstrom, E.E., *Upper critical fields in Ni- and Co- doped pnictide bulk superconductors*, submitted to *Phys. Rev B*.
34. Huan Yang, Huiqian Luo, Zhaosheng Wang, Hai-Hu Wen, *Appl. Phys. Lett*. **93**

142506 (2008).
35. D.L. Sun, Y. Liu, C.T. Lin, *Phys. Rev. B* **80** 144515, (2009).
36. Fabbricatore P, Farinon S, Gemme G, Musenich R, Parodi R and Zhang B, *Phys. Rev.* B **50** 3189 (1994).
37. Nikolo, M., Stacey, L.M. and Missey, M.J., *Solid State Comm.*, **94**, 997 (1995).
38. Shivagan, D D, et al., *Supercond. Sci. Technol.* **21**, Number 9, 095002 (2008).
39. Fisher M. P. A., *Phys. Rev. Lett.* **62** 1415 (1989).
40. Fisher D. S., Fisher, M. P. A. and Huse, D. A., *Phys. Rev.* B **43** 130 (1991).
41. Nikolo, M., Singleton, J., Zapf, V.S., Jiang J., Weiss J., and Hellstrom E., *Irreversibility line measurement and vortex dynamics in high magnetic fields in Ni- and Co-doped iron pnictide bulk superconductors,* to be submitted.